Optical Properties and Band Structure of Titanium Carbide*

ROBERT G. LYE†
Parma Technical Center, Union Carbide Corporation, Cleveland, Ohio

AND

E. M. LOGOTHETIS
Laboratory of Atomic and Solid State Physics, Cornell University, Ithaca, New York

(Received 24 February 1966)

Near-normal-incidence reflectivity measurements have been made from 0.5 to 21 eV on cleaved (100) faces of various TiC_x specimens. Optical properties determined from dispersion (Kramers-Kronig) analyses of the reflectivity have been used, together with other information from the literature, to estimate values of the band parameters for a semiempirical, tight-binding calculation of the band structure. The two-center formalism of Slater and Koster was used for this purpose, but with the integrals treated as adjustable parameters not subject to the usual restrictions of the two-center approximation. The result differs markedly from other band structures for TiC which have appeared in the literature.

I. INTRODUCTION

TITANIUM carbide is one member of a group of substances, frequently referred to as the refractory hard metals, whose unusual properties have been the subject of numerous studies[1] for several years. The simple face-centered-cubic rock-salt structure of TiC and its recent availability[2] in the form of moderately good single crystals of useful size have justified a closer examination of its properties from both the theoretical and experimental points of view in an attempt to provide a more quantitative interpretation than previously has been possible for the refractory hard metals. Many difficulties, however, remain to be surmounted: Insufficient data are available to provide an adequate characterization of the complex behavior of any of these substances and computations of their band structures involve the normal difficulties of the transition metals together with those posed by the presence of a second atom in the unit cell. For these reasons, it was decided to begin the study with a semiempirical calculation of the band structure of TiC, using whatever experimental data were available as a guide during the computations. It was apparent, however, that a valid calculation by this approach required knowledge of properties of the band structure over a range of energies far wider than that which had been studied previously. Fortunately, the advice of Professor P. L. Hartman and facilities developed by him and his group at Cornell University were made available for optical studies through the visible and into the vacuum ultraviolet region of the spectrum. Measurements of the reflectivity at near-normal incidence made under these arrangements provided significant new experimental information from which it has been possible to deduce an internally consistent energy-band structure. The result is, no doubt, subject to considerable refinement by more precise methods of calculation, but it may provide useful guidance in performing such calculations. In the meantime, this band structure indicates a need to interpret the properties of TiC in a manner somewhat different from that suggested by previous studies carried out without the benefit of the optical data presented here. In particular, the present band structure differs widely from those proposed some time ago by Bilz[3] and, more recently, by Ern and Switendick,[4] especially in regard to the position of the $2p$ bands of carbon. The discrepancy remains to be resolved and may serve to justify a more sophisticated examination of the refractory hard metals than they have received heretofore.

In Secs. II and III of this paper, the measurements of reflectivity and their interpretation are described. In Sec. IV, the band structure calculations are discussed; in Sec. V, the method used here to derive the optical properties associated with the calculated band structure is developed. In Sec. VI, the resulting band structure is considered in relation to experimental observations and compared with related work in the literature.

II. EXPERIMENTAL

A. Method

Infrared, visible, and near ultraviolet reflectivity. Measurements of the reflectivity from 0.5 to 5.6 eV were made using a Cary Model 14 recording double-beam spectrophotometer modified as described by

* Work supported in part by the Research and Technology Division, Air Force Systems Command, U. S. Air Force, and in part by the Advanced Research Projects Agency of the Department of Defense through the Materials Science Center at Cornell University.

† Present address: Research Institute for Advanced Studies (Martin Company), Baltimore, Maryland.

[1] P. Schwarzkopf and R. Kieffer, *Refractory Hard Metals* (The Macmillan Company, New York, 1953), and, more recently, R. Kieffer and F. Benesovsky, *Hartstoffe* (Springer-Verlag, Vienna, 1963) provide reviews of the subject.

[2] TiC crystals used in this study were grown by the arc-Verneuil process at Linde Division of Union Carbide Corporation. Chemical composition and other properties of these crystals have been discussed recently by W. S. Williams, Phys. Rev. **135**, A505 (1964).

[3] H. Bilz, Z. Physik **153**, 338 (1958).

[4] V. Ern and A. C. Switendick, Phys. Rev. **137**, A1927 (1965). This paper provides an adequate discussion of prior work related to the present study and an extensive list of references which will not be duplicated here.

Hartman and Logothetis.[5] Additional apertures were necessary, however, to limit the monochromator beams to the useful area (approximately 2 by 3 mm) of the small crystals available for the present study.

Vacuum ultraviolet reflectivity. The vacuum ultraviolet monochromator and light sources used to obtain the reflectivity have been described in detail by Hartman.[6,7] The ultraviolet region of the spectrum was studied in two overlapping parts: from 4.5 to 12 eV, the light intensity was measured with a phosphor converter and a photomultiplier detector; from 8 to 21 eV, the intensity was obtained by measuring the current which the light ejected from an appropriate photoemitter.

In the region from 4.5 to 12 eV, the reflectivity was determined by measuring the signal from a specially selected EMI 6097S photomultiplier under two conditions: (a) with the monochromator light reflected once from an aluminum mirror onto the center of the sodium salicylate phosphor-coated window of the photomultiplier,[8] and (b) with the light reflected from the specimen to the same aluminum mirror and then to the same part of the photomultiplier window. For the first part of the measurement, (a), the mirror was disposed as shown in Fig. 1(a) so that a horizontal line in the plane of the mirror was at the elevation of the (horizontal) light beam and perpendicular to it. The mirror was oriented about a horizontal axis to reflect the light beam onto the center of the photomultiplier window and fixed in this position relative to the photomultiplier assembly. For the second part of the measurement, (b), the photomultiplier and mirror were rotated together by 154 deg about a vertical axis through the photomultiplier and the specimen was inserted into the light beam, as shown in Fig. 1(b), with a vertical line in the plane of the specimen perpendicular to the incident beam. The specimen was oriented about a vertical axis to reflect the beam in a horizontal plane onto the mirror and from there to the photomultiplier. Under these conditions, the light was incident on the specimen at 13 deg from the normal, close enough that the normal-incidence approximation to the Fresnel relations can be employed with little error. Although smaller angles of incidence could have been achieved, the angle was maintained at 13 deg to coincide with the configuration demanded by the reflectometer used for measurements in the visible spectrum.

After being reflected by the specimen, the light traversed a path which had the same configuration relative to the mirror and photomultiplier as it had in the first measurement (a). Thus, the same region of the photomultiplier window was illuminated in both measurements, thereby avoiding effects of possible variations in the luminous efficiency of the phosphor over the photomultiplier window.

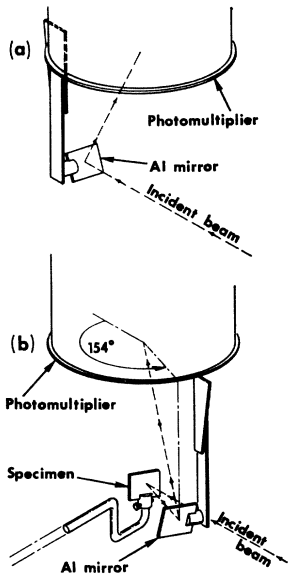

FIG. 1. Reflectometer arrangement using the EMI 6097S photomultiplier as detector; (a) with Al mirror in the direct beam, and (b) with the light reflected once from the specimen before striking the Al mirror.

The techniques employed here give a direct measurement of the absolute reflectivity of the specimen as a ratio of the photomultiplier signals in the two conditions: the aluminum mirror transfers light to the photomultiplier in the same way under both conditions and, consequently, does not influence the signal ratio. The accuracy of the method is limited, however, by the small reflectivity of aluminum above 10 eV; the signal strength is small then for both the direct beam from the aluminum mirror and for the reflected beam from the specimen. Under these conditions, the beam intensity at the photomultiplier becomes comparable in strength to the intensity of the low-energy scattered light. Since filters are not applicable in the spectral region of interest, a different method of detection was employed based on the sharply rising yield of a photoemitter above its threshold.

The use of a gold photoemitter as a detector permitted measurements to be made from 10 eV to the limit of the light source, 21 eV. The measurements were made by comparing the current ejected from the gold photoemitter under two conditions: (a) with the monochromator beam incident directly onto the gold foil, as shown in Figs. 2(a), and (b) with the light reflected from the sample (again at 13 deg from normal incidence) before striking the gold foil, as shown in Fig. 2(b). In both cases, the specimen and its mount served as collector for the photoelectrons by carrying a positive potential of 75 V, enough to collect the saturated photocurrent.

In order to provide a longer region of overlapping measurements, additional measurements were made using the photoemission technique with a thin evaporated film of AgBr as the detector instead of the gold detector previously used. Following a brief period of change after deposition, these films were stable for

[5] P. L. Hartman and E. M. Logothetis, Appl. Opt. 3, 255 (1964).
[6] P. L. Hartman, Rev. Sci. Instr. 33, 1082 (1962).
[7] P. L. Hartman, J. Opt. Soc. Am. 51, 113 (1961).
[8] K. Watanabe and C. Inn, J. Opt. Soc. Am. 43, 32 (1953).

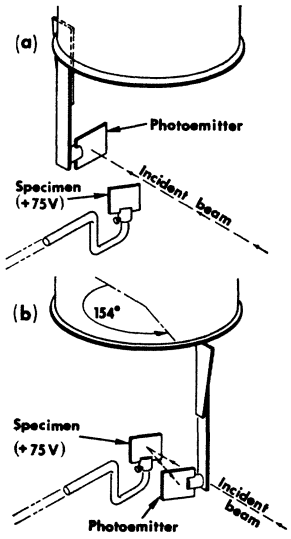

FIG. 2. Reflectometer arrangement using a gold (or AgBr) photoemission surface as detector; (a) with the photoemitter in the direct beam, and (b) with the light reflected once from the specimen before striking the photoemitter. In both configurations, the specimen and its mount were held at +75 V relative to the photoemitter to permit collecting saturated photocurrent from the detector.

several days with a sensitivity sufficient to permit measurements at energies as low as 7 eV.

Photoemission. The photoelectric yields of some crystals of TiC_x were obtained in the region above 8 eV (where the quantum yields exceeded 10^{-4} electrons per incident photon) by comparing the emission from the specimen with that of gold under the same conditions. These measurements were made by a procedure essentially the same as that used to study the reflectivity with the photoemission detector. To measure the photoemission of TiC_x, however, a nickel plate at +75 V was used as the collector with the gold foil as the emitter in one case and the TiC_x crystal as the emitter in the other.

B. Results

Available crystals of TiC are usually small with various imperfections on the (100) cleaved faces. In consequence, a portion of the incident light was lost from the reflected beam, thereby limiting the accuracy of determinations of the absolute reflectivity; various measurements obtained by removing and replacing the same crystal yielded values which differed by as much as 5% in magnitude but with no significant change in shape. Values of the reflectivity for different crystals of the same nominal composition differed somewhat more widely. The absolute reflectivity was established for one crystal ($TiC_{0.794}$) by determining the correction to its measured reflectivity necessary to account for light losses caused by surface imperfections. To do so, the apparent reflectivity of an opaque aluminum film evaporated onto the crystal face was compared with the reflectivity of a similar film evaporated onto a flat glass plate which, accordingly, was free of the geometric defects to which the crystal was subject. The apparent reflectivity of the film on the crystal was smaller than that on the glass plate by a constant factor (16%), uniform over the region measured (0.5 to 5.8 eV). When the apparent reflectivity of the crystal in the low-energy region was corrected by the appropriate multiplying factor, it was possible, also, because of the extensive overlap between regions studied by different methods, to extend the absolute-reflectivity curve for the crystal to 21 eV.

The other crystals were treated in the same way with the additional assumption that the reflectivity in the low-energy region (0.5 to 5.8 eV) was the same for all the crystals studied. The assumption is not unreasonable, since the room temperature resistivity of each crystal is expected to fall within the limits 160–200 $\mu\Omega$ cm; thus, the Hagen-Rubens relation may be used to show that their infrared reflectivities should be within approximately 2% of the same value, that is, within the remaining experimental uncertainties. Although the Hagen-Rubens relation is not rigorously applicable in the region of experimental observation, the more accurate expression,

$$R=1-(2\omega/\pi\sigma_0)^{1/2}[(1+\omega^2\tau^2)^{1/2}-\omega\tau]^{1/2}, \qquad (1)$$

developed by Bennett, Silver, and Ashley,[9] provides the same result so long as the mean free time τ does not vary rapidly with composition. Studies of resistivity and Hall effect[2] and thermoelectric power[10] provide evidence that τ varies rapidly with carbon content for $x=[C]/[Ti]\gtrsim 0.93$ but more slowly for $x\lesssim 0.93$. Thus, the absolute reflectivity of the crystals studied here is probably close to the value determined if one assumes that all have the same reflectivity in the low-energy region as the crystal $TiC_{0.794}$; for more nearly stoichiometric crystals, however, it is expected

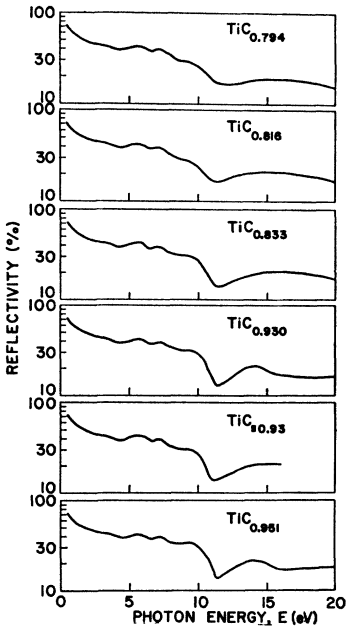

FIG. 3. Reflectivity of TiC_x crystals at 13 deg from normal incidence.

[9] H. E. Bennett, M. Silver, and E. J. Ashley, J. Opt. Soc. Am. 53, 1089 (1963).
[10] R. G. Lye, J. Phys. Chem. Solids 26, 407 (1965).

that differences would be observed in the infrared region because of variations of the mean free time for such crystals.

Under these assumptions, the curves given in Fig. 3 represent the absolute reflectivities of TiC_x crystals from 0.5 to 21 eV.[11] Each curve shown is the average of two or more separate measurements and has been confirmed by additional measurements on a second sample of the same composition. The variation of the reflectivity with carbon content is particularly pronounced near 11 eV, but lesser variations are detectable from 6 to 15 eV.

Although the accuracy of individual measurements remains high, the number of spectral lines useful for measuring the reflectivity is small in the region from 15 to 21 eV. Smooth curves drawn through these points are given in Fig. 3; additional, unobserved structure may be present, however, in the region above 15 eV.

Photoemissive yields were measured for three of the larger crystals of TiC_x. In order to emphasize the dependence of their photoemission on carbon content, the unmodified experimental data are plotted as the yield relative to the yield of gold, $\eta_x/\eta_{\text{gold}}$, in Fig. 4. Differences between the yield curves from $TiC_{0.95}$ and $TiC_{0.93}$ may not be important, but a pronounced qualitative difference in shape is apparent between each of these and the curve for $TiC_{0.794}$. It appears, then, that the photoemission has a composition-dependent component centered in a peak between 10 and 11 eV.

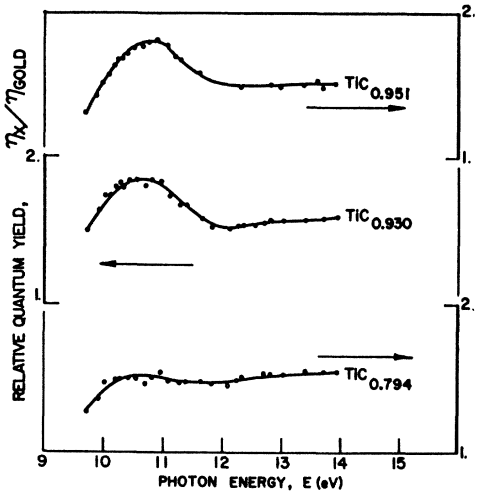

FIG. 4. Photoemission of TiC_x crystals measured relative to the photoemission of gold.

[11] Measurements were made also of the reflectivity of zirconium carbide and niobium carbide crystals and of titanium and zirconium metals. The results are described by E. M. Logothetis, M.S. thesis, Cornell University, 1965 (unpublished) and by W. S. Williams and R. G. Lye, Technical Documentary Report ML-TDR-64-25, Part II, 1965, from Air Force Materials Laboratory, Research and Technology Division, Air Force Systems Command, Wright-Patterson Air Force Base, Ohio (unpublished). The latter report is available to qualified requesters from the Defense Documentation Center as Publication AD-463, 115.

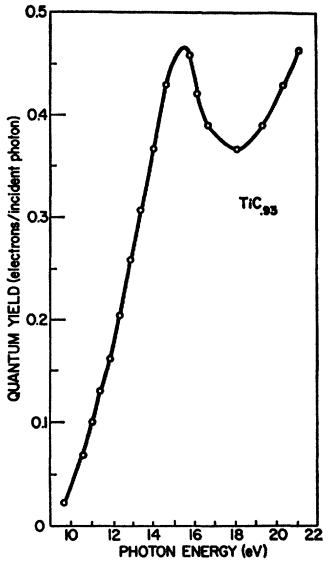

FIG. 5. Absolute photoelectric yield of $TiC_{0.93}$ obtained from the data plotted in Fig. 4 by using Lloyd's curves (Ref. 12) for the absolute photoelectric yield of gold.

The absolute photoemission was calculated from the relative yield shown in Fig. 4 by using Lloyd's[12] data for the absolute photoemission of gold. Although the experimentally definite structure between 10 and 11 eV is no longer prominent in the sharply rising absolute photoyield of $TiC_{0.93}$, shown in Fig. 5, a new peak has become obvious near 15 eV. Similar calculations with the yield or other crystals suggest that the intensity of the 15-eV peak also may be composition-dependent, but the evidence is not conclusive.

III. ANALYSIS OF REFLECTIVITY

The reflectivity of crystal $TiC_{0.951}$ was extrapolated[13] at its 21-eV value to higher energies and along a smooth curve to $R=1$ at low energies. Kramers-Kronig analyses[14] of the resulting curve were performed, using conventional computing techniques, to obtain the optical constants for this crystal.

The real and imaginary parts of the dielectric constant $\epsilon=\epsilon_1+i\epsilon_2$, obtained in this way are shown in Fig. 6. The frequency-dependent conductivity (optical conductivity), $\sigma=\omega\epsilon_2/4\pi$, which is discussed later, is shown in Fig. 7. Its integral,

$$\int_0^{\omega_0}\omega\epsilon_2 d\omega=(2\pi^2Ne^2/m)n_1(\omega_0)\,, \qquad (2)$$

[12] J. N. Lloyd, Ph.D. thesis, Cornell University, 1963 (unpublished).

[13] These arbitrary extensions of the experimental data introduce uncertanties to the results of the analysis, but the effects appear not to be serious within the measured spectral region. Different extrapolations based on an inverse power of the photon energy $R\alpha\omega^{-p}$, for $\hbar\omega>21$ eV were compared, but the results were physically reasonable only for the exponent near zero.

[14] Application of Kramers-Kronig analyses to the present problem depended primarily on prior exploitation of the technique by H. R. Philipp and E. A. Taft, Phys. Rev. **113**, 1002 (1959), and by H. Ehrenreich, H. R. Philipp, and B. Segall, *ibid.* **132**, 1918 (1963).

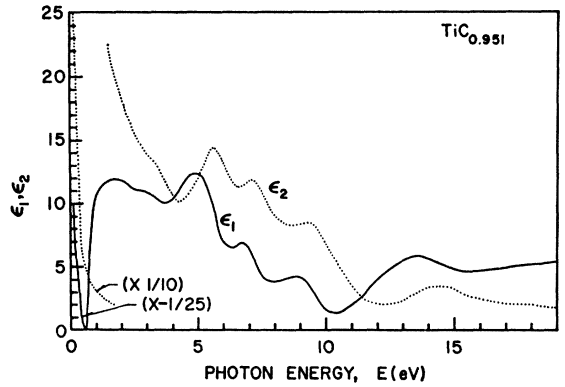

FIG. 6. The (experimental) real and imaginary parts of the dielectric constant, $\epsilon=\epsilon_1+i\epsilon_2$, of $TiC_{0.951}$ obtained by Kramers-Kronig analysis of the reflectivity curve shown in Fig. 3. At small energies, $-\epsilon_1/25$ and $\epsilon_2/10$ are plotted.

is proportional to the effective number of free electrons, $n_1(\omega_0)$, per molecule of TiC contributing to the optical properties in the range 0 to ω_0 (m is the free electron mass and N is the number of molecules of TiC per unit volume); $n_1(\omega_0)$ is given in Fig. 8.

The number of optically active electrons given by $n_1(\omega)$ reaches a plateau near 11 eV at a value of approximately six electrons per molecule. The result may be taken as evidence that this group of six electrons is separated in energy from lower lying groups of electrons: intuitively, the six electrons are expected to be the upper four of titanium and the upper two of carbon. If the energy separation were more extensive, these electrons could be expected to behave essentially as free electrons having a plasma frequency near the asymptotic value given by[15] $\omega_p^2=4\pi Ne^2/m$, which yields $\hbar\omega_p=20.3$ eV for $n=6$ electrons per molecule, and to generate a dielectric constant similar to that given by the Drude relation,[16] $\epsilon(\omega)=1-\omega_p^2/\omega(\omega+i/\tau)$. This almost free-electron behavior is seen in ϵ_1 and ϵ_2 (Fig. 6) over a narrow interval around 11 eV. The continued rise in $n_1(\omega)$ above 11 eV implies, however, that other electrons (carbon 2s electrons) become optically active at only slightly higher energies; and, thus, the associated interband transitions are expected to depress[17] the plasma frequency from its asymptotic value. The behavior suggested by this argument appears to be well demonstrated in Fig. 9, which shows the loss function, $-\mathrm{Im}\epsilon^{-1}=\epsilon_2/(\epsilon_1^2+\epsilon_2^2)$; a prominent peak which satisfies the conditions[18] necessary to attribute it to a plasma excitation is observed near $\hbar\omega_k=11$ eV, well below the calculated energy, $\hbar\omega_p=20.3$ eV. The number, $n_2(\omega_0)$, of optically active electrons contributing to the loss function is given by Eq. (3) and is shown in Fig. 8.

$$\int_0^{\omega_0} -\omega\,\mathrm{Im}\epsilon^{-1}d\omega=(2\pi^2Ne^2/m)n_2(\omega_0)\,. \qquad (3)$$

The number of these electrons contributing to the plasma resonance is small, however, presumably because of the shielding effect of the lower lying electrons; n_2 changes by only 0.05 electrons per molecule over the width of the peak. The relaxation time of the electrons contributing to the 11-eV resonance, $\tau=3.2\ 10^{-16}$ sec, as determined from the lifetime of the plasma oscillation[19] ($\Delta\omega/\omega_k=2/\omega_p\tau$), is comparable to values found for the relaxation time of electrons in valence bands of semiconductors ($1.4-1.8\times10^{-16}$ sec)[19] and is much smaller than for electrons in the conduction bands of copper and silver[20] ($\cong10^{-14}$ sec). This relaxation time in TiC probably is determined, then, as in the semiconductors, primarily by electron-electron interactions rather than by electron-phonon or electron-impurity scattering. Unfortunately, the simple metallic (Drude) behavior of the conduction electrons in TiC is not observable in the spectral region accessible for our measurements. Consequently, it was not possible to determine from optical measurements the mean free time and effective mass of the electrons responsible for the transport properties of TiC.

IV. ENERGY-BAND CALCULATIONS

The band structure was calculated in the tight-binding approximation following the well-known approach of Slater and Koster[21] and using their two-center formalism. Matrix components of the secular equation appropriate for the fcc rock-salt lattice of TiC were taken from Table III of Slater and Koster using

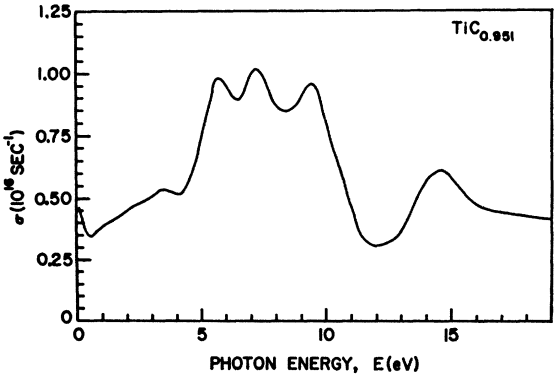

FIG. 7. The (experimental) frequency-dependent conductivity, $\sigma=\omega\epsilon_2/4\pi$, for $TiC_{0.951}$ obtained by analysis of the reflectivity curve shown in Fig. 3.

[15] The corresponding situation in aluminum has been discussed by Ehrenreich *et al.* (Ref. 14).

[16] S. Roberts, Phys. Rev. **118**, 1509 (1960).

[17] C. B. Wilson, Proc. Phys. Soc. (London) **76**, 481 (1960).

[18] H. Ehrenreich and H. R. Philipp, *Proceedings of the International Conference on the Physics of Semiconductors, Exeter* (The Institute of Physics and the Physical Society, London, 1962), p. 367 ff.

[19] H. R. Philipp and H. Ehrenreich, Phys. Rev. **129**, 1550 (1963).

[20] H. Ehrenreich and H. R. Philipp, Phys. Rev. **128**, 1622 (1962).

[21] J. C. Slater and G. F. Koster, Phys. Rev. **94**, 1498 (1954).

TABLE I. Atomic orbitals (or Löwdin sums of atomic orbitals) employed in the energy-band calculations, their sequence in the eigenfunctions, and the abbreviations used to describe them. (Imaginary p functions were used so that only real components would be present in the Hamiltonian and in the eigenvectors. The coordinate axes are directed from an atom of one kind to nearest neighbors of the opposite kind.)

(1)	carbon 2s-like functions, abbreviated	sA
(2)	$2p_x$	xA
(3)	$2p_y$	yA
(4)	$2p_z$	zA
(5)	titanium 4s-like functions, abbreviated	sM
(6)	$4p_x$	xM
(7)	$4p_y$	yM
(8)	$4p_z$	zM
(9)	$3d_{xy}$	xyM
(10)	$3d_{yz}$	yzM
(11)	$3d_{zx}$	zxM
(12)	$3d_{(x^2-y^2)}$	$(x^2-y^2)M$
(13)	$3d_{(3z^2-r^2)}$	$(3z^2-r^2)M$.

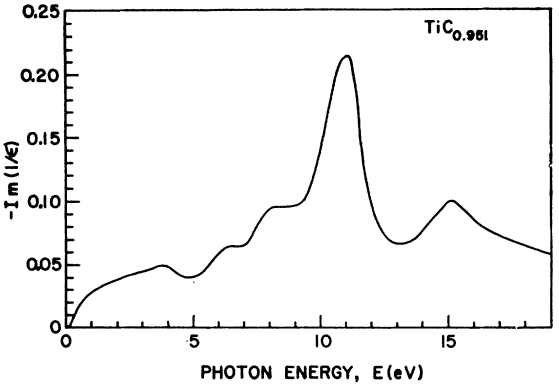

FIG. 9. The (experimental) loss function, $-\mathrm{Im}\epsilon^{-1}=\epsilon_2/(\epsilon_1^2+\epsilon_2^2)$, for $TiC_{0.951}$ obtained by Kramers-Kronig analysis of the reflectivity curve shown in Fig. 3.

only nearest- and next-nearest neighbor two-center integrals. Computer solutions of the equation provided the coefficients, $c(i,j)$, of the ith component of the jth eigenfunction, and the energy of that eigenfunction, at selected points in the Brillouin zone. To simplify subsequent discussion, the order of the components of the wave functions and the abbreviations used to describe them are listed in Table I.

The two-center formalism was used throughout the calculation, but the parameters representing the two-center integrals were considered to be free of the restrictions[21] which accompany strict application of the two-center approximation in order to allow, in part, for the effects of three-center interactions which Costa and Conte[22] have shown to be important in TiC. Thus, these parameters were estimated initially by reference to the studies of Bilz[3] and of Costa and Conte[22]; subsequently, they were adjusted freely to generate band characteristics which were consistent with the observed optical properties.

Preliminary estimates of the relative positions of the bands in the carbide were obtained, following Bilz, from the differences s_{0A}, p_{0A}, s_{0M}, p_{0M}, and d_{0M} between the one-electron energies of the corresponding states of the atoms and the one-electron energy for the $3d$ states of titanium. Bilz, however, used for the $2p$ states the average of the one-electron energies of carbon, nitrogen, and oxygen and obtained thereby a band structure which he suggested might be used to represent all three compounds TiC, TiN, and TiO. In the present calculation, the one-electron energies of atomic carbon $2p$ states were used alone so as to make the band structure apply more specifically to TiC. The first results led, as in Bilz's calculation, to an unreasonably large transfer of electrons from titanium $3d$ states to carbon $2p$ states. Accordingly, an electrostatic correction was applied to raise the carbon $2p$ states until the charge transfer was approximately consistent with the Madelung displacement of the energy levels. Subsequently, however, these energy parameters were also adjusted to match the band structure to the observed optical properties.

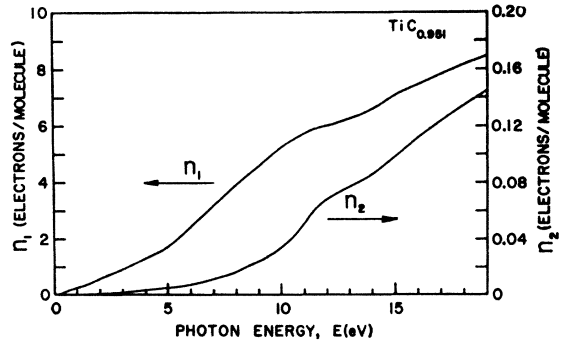

FIG. 8. The (experimental) number of optically active electrons per molecule of $TiC_{0.951}$, $n_1(E)$ and $n_2(E)$, obtained from the integral [Eq. (2)] of the optical conductivity and from the integral [Eq. (3)] of the loss function, respectively.

Band structures obtained from these calculations for various combinations of the energy parameters were tested primarily by comparing the optical conductivity derived from them (see next section) with the conductivity obtained by dispersion analysis of the reflectivity. Additional adjustments of certain parameters were made to satisfy other experimental observations on the Hall effect, thermoelectric power, magnetic susceptibility, and photoemission. The degree to which the final band structure satisfies the experimental data will be discussed in Sec. VI. When other information was lacking, the wave functions of the atoms given by Herman and skillman[23] were used to provide estimates of the relative magnitudes of the two-center integrals. With these tentative values for the band parameters, a band structure was calculated and compared with experimental observations; and the parameters were

[22] P. Costa and R. R. Conte in *Nuclear Metallurgy Symposium* (Metallurgical Society of AIME, New York, 1964), Vol. 10, p. 3.

[23] F. Herman and S. Skillman, *Atomic Structure Calculations* (Prentice-Hall, Inc., Englewood Cliffs, New Jersey, 1963).

adjusted to improve the agreement. When the principal requirements appeared to have been satisfied by this means, a final test was made by calculating the band structure on a closely spaced set of points uniformly distributed through the Brillouin zone (505 points in the representative[24] 1/48 of the Brillouin zone which are equivalent to 16 384 points in the full zone). From the information so obtained, a conductivity histogram was determined which was sufficiently free of sampling errors[25] that it could be compared, more or less quantitatively, with the corresponding curve obtained from the reflectivity.

V. OPTICAL-CONDUCTIVITY CALCULATIONS

At a given point k in the Brillouin zone, radiation with its electric vector in the x direction excites contributions to the optical conductivity, $\sigma_x(i-j, k)$, from band i (below the Fermi level) to band j (above the Fermi level) which can be written[26] as

$$\sigma_x(i-j, k)=(Ne^2/4m)f_x(i-j, k)\delta(\omega_{ij}-\omega), \quad (4)$$

where N is the number of TiC molecules per unit volume and $f_x(i-j, k)$ is the oscillator strength per molecule for the transition, which has the frequency ω_{ij}. The oscillator strength for the transition can be estimated using either[27] momentum matrix elements, $f_x(i-j, k)=(2/m\hbar\omega_{ij})|(\psi_j|p_x|\psi_i)|^2$, or dipole matrix elements, $f_x(i-j, k)=(2m\omega_{ij}/\hbar e^2)|(\psi_j|ex|\psi_i)|^2$, where the ψ's represent the values of the crystal wave functions at k. The geometric mean of these two expressions is more convenient for present purposes because it does not involve explicitly the initially unknown energy gaps, $\hbar\omega_{ij}$; thus, $f_x(i-j, k)=(2/e\hbar)|(\psi_j|ex|\psi_i)|\times|(\psi_j|p_x|\psi_i)|$.

To employ this approach, operators Q_x, Q_y, and Q_z, which do not explicitly involve the energy gaps, are defined so that the square of the matrix element between Q_x and two Bloch functions gives directly the oscillator strength for the electric vector in the x direction, $f_x(i-j, k)=|(\psi_j|Q_x|\psi_i)|^2$. For these new operators, the assumption is made that their matrix elements can be represented in the same way as common one-center or two-center dipole matrix elements. Thus, the relations given in Table II at once define the matrix elements I_S, I_D, I_P, I_C, and I_T and describe the dipole approximation they are supposed to satisfy.[28] In the following discussion, these matrix elements will be considered to be adjustable parameters which are chosen to provide optimum agreement with the observed optical properties.

TABLE II. Definitions of optical matrix elements.

I. For the electric vector in the [100] direction and for the two atoms connected by a lattice vector in the same direction:

$$\begin{gathered}(sM|Q_x|xA)=I_S\\((x^2-y^2)M|Q_x|xA)=\tfrac{1}{2}\sqrt{3}I_D\\((3z^2-r^2)M|Q_x|xA)=-\tfrac{1}{2}I_D\\(sA|Q_x|xM)=I_P\\(sA|Q_x|xA)=I_C\\(sM|Q_x|xM)=I_T.\end{gathered}$$

The two-center integrals involving p_y and p_z functions vanish, as do integrals involving atoms connected by lattice vectors other than [100].

II. For the electric vector in the [010] direction and for the two atoms connected by a lattice vector in the same direction:

$$\begin{gathered}(sM|Q_y|yA)=I_S\\((x^2-y^2)M|Q_y|yA)=-\tfrac{1}{2}\sqrt{3}I_D\\((3z^2-r^2)M|Q_y|yA)=-\tfrac{1}{2}I_D\\(sA|Q_y|yA)=I_C\\(sM|Q_y|yM)=I_T.\end{gathered}$$

The two-center integrals involving p_x and p_z functions vanish, as do integrals involving atoms connected by lattice vectors other than [010].

III. For the electric vector in the [001] direction and for the two atoms connected by a lattice vector in the same direction:

$$\begin{gathered}(sM|Q_z|zA)=I_S\\((x^2-y^2)M|Q_z|zA)=0\\((3z^2-r^2)M|Q_z|zA)=I_S\\(sA|Q_z|zM)=I_P\\(sA|Q_z|zA)=I_C\\(sM|Q_z|zM)=I_T.\end{gathered}$$

The two-center integrals involving p_x and p_y functions vanish, as do integrals involving atoms connected by lattice vectors other than [001].

In terms of these parameters, the oscillator strengths for the electric vector in the three perpendicular directions become

$$\begin{aligned}f_x&=\{2\cos\xi[a_xI_S+b_xI_D+c_xI_P]+2[d_xI_C+e_xI_T]\}^2,\\f_y&=\{2\cos\eta[a_yI_S+b_yI_D+c_yI_P]+2[d_yI_C+e_yI_T]\}^2, \quad (5)\end{aligned}$$

and

$$f_z=\{2\cos\zeta[a_zI_S+b_zI_D+c_zI_P]+2[d_zI_C+e_zI_T]\}^2,$$

where the abbreviations $\xi=ak_x$, $\eta=ak_y$, and $\zeta=ak_z$ are used with a representing the nearest-neighbor interatomic distance and the coefficients of the matrix elements are evaluated from the solution of the tight-binding calculation of the band structure discussed in Sec. IV. The quantities a, b, c, d, e are computed from quantities C, which are defined in terms of the coef-

[24] Calculations of the energy band structure of copper by G. A. Burdick, Phys. Rev. **129**, 138 (1963) were used as a guide for this part of the program.

[25] D. Brust, Phys. Rev. **134**, A1337 (1964), has discussed the question of sampling errors and the results of smoothing the histogram by averaging over three adjoining intervals. The smoothing procedure was followed here also.

[26] F. Stern, in *Solid State Physics*, edited by F. Seitz and D. Turnbull (Academic Press Inc., New York, 1963), Vol. 15, p. 299 ff.

[27] F. Seitz, *Modern Theory of Solids* (McGraw-Hill Book Company, Inc., New York, 1940), p. 648.

[28] The first three of these parameters, I_S, I_D, and I_P, represent two-center integrals over nearest neighbors. The other two, I_C and I_T, represent integrals over a single atom, carbon or titanium, respectively. The approximation specified by Table I is probably rather good for I_S and I_D, since the $2p$ functions are small at nearest neighbor distances and, as can be shown by a simple calculation, the matrix elements are consequently almost proportional to the dipole matrix elements. The approximation may not be so good for I_P but will be retained for simplicity. The approximation is valid for I_C and I_T, since these are essentially one-center integrals.

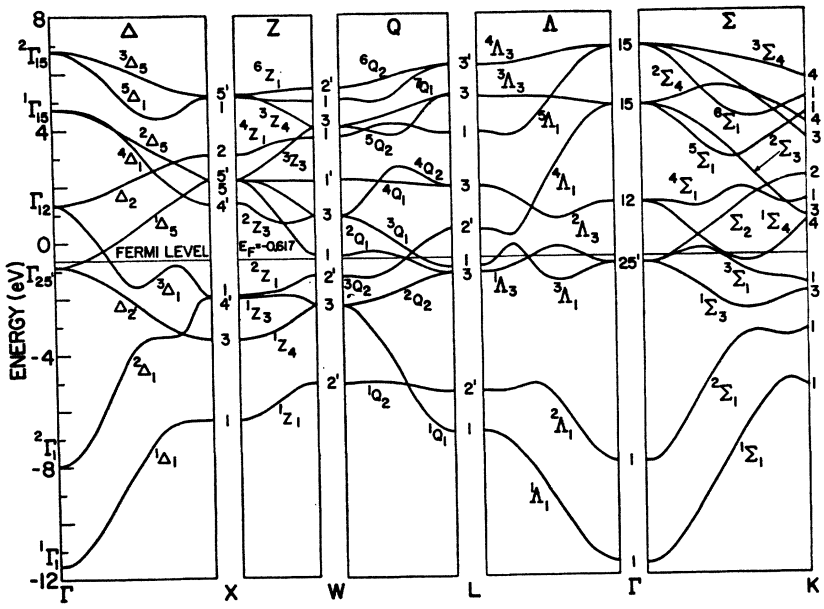

FIG. 10. Energy bands for TiC in the simplified tight-binding approximation.

ficients of the eigenfunction by $C_{m,n}(i-j)=c(m,i)c(n,j)+c(m,j)c(n,i)$. In the following equations, the band indices i and j are suppressed:

$$\begin{aligned} a_x&=C_{2,5} & b_x&=\tfrac{1}{2}\sqrt{3}C_{2,12}-C_{2,13} \\ a_y&=C_{3,5} & b_y&=-\tfrac{1}{2}\sqrt{3}C_{3,12}-C_{2,13} \\ a_z&=C_{4,5} & b_z&=C_{4,13} \end{aligned} \tag{6a}$$

$$\begin{aligned} c_x&=C_{6,1} & d_x&=C_{2,1} & e_x&=C_{6,5} \\ c_y&=C_{7,1} & d_y&=C_{3,1} & e_y&=C_{7,5} \\ c_z&=C_{8,1} & d_z&=C_{4,1} & e_z&=C_{8,5}. \end{aligned} \tag{6b}$$

The total optical conductivity, $\sigma(\omega)$, is obtained by integrating over the Brillouin zone and summing over all pairs of bands for which the lower state is below and the upper state is above the Fermi level. In terms of the mean oscillator strength $f(i-j,k)=\frac{1}{3}(f_x+f_y+f_z)$, the conductivity for an isotropic solid can be written as

$$\sigma(\omega)=\frac{Ne^2}{4m}\sum_{i,j}\int_{BZ}\frac{2f(i-j,k)\delta(\omega_{ij}-\omega)d^3k}{(2\pi)^3}. \tag{7}$$

In practice, however, the computation is carried out over the discrete set of 505 points in the representative 1/48 of the Brillouin zone for which the band structure had been evaluated, as discussed in the preceding section. At each such point, the energy gaps and oscillator strengths[29] were determined for all possible transitions, the transitions were sorted according to their energy, the oscillator strengths were weighted according to the number of "like" points[24] in the full zone, and a smoothed[25] 0.2-eV histogram was constructed of the weighted oscillator strengths. The resulting histogram provides a representation of the optical conductivity characteristic of the calculated band structure; the cumulative sum of the histogram provides a representation of the number of optically active electrons, $n_1(\omega)$, which can be compared with the experimentally derived quantity shown in Fig. 8.

VI. RESULTS AND DISCUSSION

Figure 10 shows the energy bands for certain symmetry directions in the Brillouin zone of TiC deduced from the iterative calculation discussed in Sec. IV using the values for the band parameters which are given in Table III. The bands are labeled using the standard BSW[30–32] notation with a prefixed superscript to indicate the sequence of bands of a given type, starting in each case from the band at lowest energy. The result is subject to further substantiation and refinement, but it does satisfy the demands of much of the experimental data presently available and provides a tentative basis for interpreting the properties of TiC.

[29] Unlike the circumstances which Brust (Ref. 25) found to obtain with Ge and Si, the matrix elements for the principal transitions in TiC do vary markedly through the Brillouin zone. In consequence, it was necessary in the present work to calculate the oscillator strengths, not just the joint density of states for the transition.

[30] L. P. Bouckaert, R. Smoluchowski, and E. Wigner, Phys. Rev. **50**, 58 (1936).

[31] H. Jones, *The Theory of Brillouin Zones and Electronic States in Crystals* (North-Holland Publishing Company, Amsterdam, 1960).

[32] The symmetry labels are assigned for the metal atom at the origin. A. C. Switendick, Solid State and Molecular Theory Group, Massachusetts Institute of Technology, Quarterly Progress Report No. 49, 1963, p. 41 (unpublished), has shown that the symmetries at L, W, and Q depend on which atom is chosen to be the origin of coordinates. P. M. Scop, Solid State and Molecular Theory Group, Massachusetts Institute of Technology, Quarterly Progress Report No. 54, 1964, p. 15 (unpublished), has discussed the problem for AgCl and AgBr.

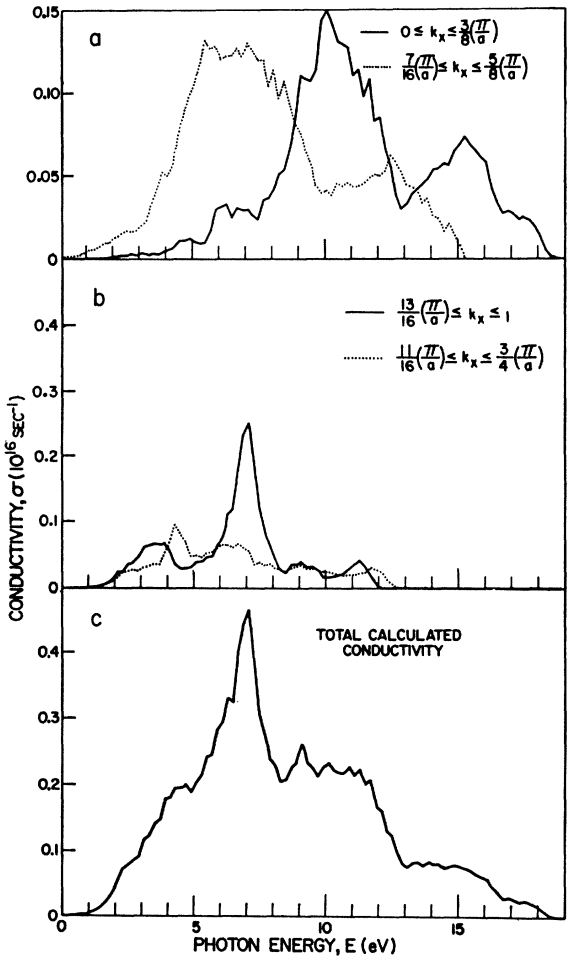

FIG. 11. Optical conductivity of TiC calculated from the band structure illustrated in Fig. 10 by using for the optical matrix elements (Table II) the values $I_S=1$, $I_P=I_D=\frac{1}{4}$, and $I_C=I_T=0$. Separate contributions are shown in (a) and (b) for regions of the Brillouin zone divided by sections parallel to the square faces at $\frac{3}{8}$, $\frac{5}{8}$, and $\frac{3}{4}$ the distance from Γ to X, i.e. near values of $|k|$ for which important oscillator strengths were found to change abruptly.

A. Optical Conductivity

According to the present result, the optical conductivity spectrum arises in a simple way: the more prominent features of the spectrum arise primarily from transitions between occupied $4s$ and vacant $2p$ states ($4s$-$2p$ transitions), between occupied $2s$ and vacant $4p$ states ($2s$-$4p$ transitions), and between occupied $2p$ and vacant $4s$ states ($2p$-$4s$ transitions). In each case, the location and shape of the resulting peaks are determined by both the joint density of states and by the variation of the oscillator strength through the Brillouin zone.

In order to emphasize the origin of structure in the conductivity spectrum, separate contributions were calculated for regions of the Brillouin zone divided by sections parallel to the square faces near values of

TABLE III. Values of parameters used in band-structure calculations for TiC (in eV).

s_{0A}	−5.000	$(ss\sigma)_A$	−0.400	$(ss\sigma)_M$	−0.870	$(ss\sigma)_{AM}$	−0.300
s_{0M}	0.720	$(sp\sigma)_A$	0.420	$(sp\sigma)_M$	0.560	$(sp\sigma)_{AM}$	0.420
p_{0A}	2.330	$(pp\sigma)_A$	0.880	$(pp\sigma)_M$	0.880	$(sp\sigma)_{MA}$	0.625
p_{0M}	4.100	$(pp\pi)_A$	−0.094	$(pp\pi)_M$	−0.150	$(pp\sigma)_{AM}$	0.560
d_{0M}	0.000			$(sd\sigma)_M$	−0.720	$(pp\pi)_{AM}$	−0.080
				$(pd\sigma)_M$	−0.600	$(sd\sigma)_{AM}$	−0.500
				$(pd\pi)_M$	0.300	$(pd\sigma)_{AM}$	−0.800
				$(dd\sigma)_M$	−0.650	$(pd\pi)_{AM}$	0.300
				$(dd\pi)_M$	0.550		
				$(dd\delta)_M$	−0.220		

$|k|$ for which the oscillator strengths change rapidly. These regions of the full zone are defined by divisions of the representative 1/48 of the zone at $k_x=\frac{3}{8}(\pi/a)$, $\frac{5}{8}(\pi/a)$ and $\frac{3}{4}(\pi/a)$, where k_x is measured along the line Γ-X.

Figure 11 shows the conductivity calculated for points uniformly distributed through the Brillouin zone with a grid spacing $\frac{1}{16}$ the distance Γ-X (16 384 points in the full zone). The curves shown were obtained by using for the optical matrix elements the values $I_S=1$, $I_P=I_D=\frac{1}{4}$, and $I_C=I_T=0$; the curves, however, do not appear to be highly sensitive to the magnitudes of I_D, I_C, or I_T.

The solid curve in Fig. 11(a) shows contributions from the region $0\leqq k_x\leqq\frac{3}{8}(\pi/a)$, in which the strong peak near 10 eV is due to $4s$-$2p$ transitions between occupied $4s$-like states associated with $^2\Gamma_1$ and vacant $2p$-like states associated with $^1\Gamma_{15}$. The oscillator strengths for transitions to two of the upper $2p$ states, those connected to $^5\Sigma_1$ and to $^2\Sigma_4$, decrease abruptly for $|k|\gtrsim\frac{3}{8}(\pi/a)$ causing a decline in the conductivity on the low-energy side.

The third $4s$-$2p$ transition, for which the upper states are connected to $^2\Sigma_3$, remains strong far out into the Brillouin zone where the band gap is considerably smaller than it is at Γ and then decreases abruptly for $|k|\gtrsim\frac{5}{8}(\pi/a)$. The dashed curve in Fig. 11(a), which is the contribution from $\frac{7}{16}(\pi/a)\leqq k_x\leqq\frac{5}{8}(\pi/a)$, exhibits the strong peak near 6 eV because of such transitions.

The $2s$-$4p$ transitions behave in much the same way as do the $4s$-$2p$ transitions: the peak near 15 eV in the solid curve of Fig. 11(a) is due to transitions from occupied $2s$-like states associated with $^1\Gamma_1$ to vacant $4s$-like states associated with $^2\Gamma_{15}$. A decline of the oscillator strengths for transitions to states connected to $^6\Sigma_1$ and to $^3\Sigma_4$ causes a corresponding decrease in the conductivity on the low-energy side. The third $2s$-$4p$ transition remains strong farther from the center of the zone and contributes significantly to the peak near $12\frac{1}{2}$ eV in the dashed curve of Fig. 11(a).

The peak near $7\frac{1}{4}$ eV in the solid curve of Fig. 11(b) arises from transitions near the square face, $\frac{13}{16}(\pi/a)\leqq k_x\leqq(\pi/a)$, between occupied $2p$-like states and vacant $4s$-like states. According to the present band structure, the lower states of this transition are associated primarily with the energy surface connected to $^2\Delta_1$, and

the upper states are associated with $^5\Delta_1$. However, occupied $2p$ states are associated also with the surface connected to $\Delta_{2'}$ and the $7\frac{1}{4}$-eV peak, accordingly, receives contributions also from transitions like $\Delta_{2'}$-$^5\Delta_1$. Matrix elements for the $2p$-$4s$ transitions are large only for a narrow section near the square face; consequently, the $7\frac{1}{4}$-eV peak too, is influenced strongly by both the variation of the oscillator strength and by the variation of the joint density of states.

The dashed curve of Fig. 11(b) shows the conductivity arising from transitions in the region $\frac{11}{16}(\pi/a) \leqq k_x \leqq \frac{3}{4}(\pi/a)$; contributions are present from each of the important transitions, but no priminent structure is evident.

Structure in the conductivity spectrum below 5 eV arises primarily from $4s$-$2p$ transitions associated with a critical point near $k=(\frac{1}{2},\frac{3}{16},\frac{3}{16})(\pi/a)$ for transitions like $^3\Delta_1$-$^2\Delta_5$, but much of the conductivity arises from the region around $k=(\frac{5}{8},0,0)(\pi/a)$ because of a maximum in the oscillator strength for the transition near this point.

The energy surface connected to $^3\Delta_1$ has appreciable $3d$-character in the outer regions of the zone, with the result that $3d$-$2p$ (as well as $4s$-$2p$) transitions contribute to the oscillator strength at low energies for transitions like $^3\Delta_1$-$^2\Delta_5$. The $3d$-$2p$ transitions are weak, however, and have not been examined in detail. Preliminary studies suggest that $3d$-$4p$ transitions also contribute to the conductivity in this low-energy region, but, because they appear not to have a pronounced effect, they will not be considered further in the present approximation.

The very low frequency and dc conductivity have not been considered here because of the lack of experimental information in the far-infrared region and the lack of adequate precision in the calculated band structure near the Fermi level.

Neither the absolute values nor the relative magnitudes of the optical matrix elements have been adjusted carefully at the present stage of the study. Nevertheless, the calculated conductivity exhibits in Fig. 11(a) and 11(b) three peaks of different origins which can be correlated with the three prominent peaks near 6 eV, $7\frac{1}{4}$ eV, and $9\frac{1}{2}$ eV in the experimental conductivity shown in Fig. 7. Appropriate changes of the optical matrix elements can be expected to modify the shapes of the calculated peaks and improve agreement of the total calculated conductivity with the experimental conductivity. Furthermore, the magnitude of the calculated conductivity, and of its integral (Fig. 12), could be made to agree better with the experimental magnitude if all the optical matrix elements used in the calculation were simply doubled. Thus, it appears possible, by minor adjustment of parameters, to generate from the calculated band structure an optical conductivity which would be in substantial agreement with the experimental curve. The question is not completely resolved, however, since the two $4s$-$2p$ peaks in Fig. 11(a) are sufficiently wide that they overlap appreciably

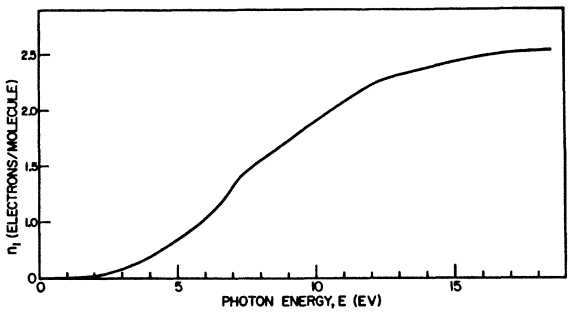

FIG. 12. The number of optically active electrons per molecule of TiC, $n_1(E)$, determined from the calculated optical conductivity of Fig. 11(c).

near $7\frac{1}{4}$ eV where the $2s$-$4p$ peak of Fig. 11 (b) also falls, thereby distorting the calculated curve. It is not certain that the breadth of the $4s$-$2p$ peaks can be reduced adequately by adjustment of the optical matrix elements alone. The origin of the excessive breadth may, in fact, imply deficiencies in the upper portion of the energy-band structure: the linear combination of atomic orbitals (LCAO) method may not provide a sufficiently precise representation of the bands at energies several electron-volts above the Fermi level. Clarification of the problem will require additional detailed examinations of both the band structure and the optical matrix elements.

B. Photoemission

Calculation of the oscillator strengths for the optical conductivity has shown that transitions from occupied $4s$-states connected with $^2\Gamma_1$ to $2p$ states connected with $^1\Gamma_{15}$ have a high probability. Externally observed photoemission should be possible for these excitations, therefore, since the level $^1\Gamma_{15}$ falls 1.3 eV above the vacuum level, which is at approximately +3.5 eV [33] in Fig. 10. This photoemission should exhibit a threshold at the band gap for which the upper states of the transition are intersected by the vacuum level. The band gap is a function of position in the Brillouin zone and, thus, the threshold is expected to be diffuse with a weak contribution extending down to approximately 7.2 eV. The emission should rise from this threshold to a maximum and then fall to zero again at a photon energy equal to the band gap at the center of the zone, 12.6 eV for the transition $^2\Gamma_1$-$^1\Gamma_{15}$. The observed behavior, shown in Fig. 4, agrees well with these predictions. This component of the photoemission is expected to decrease as carbon is removed from the TiC lattice because of the resultant decrease in the density of terminal states for the transition. It appears likely that this mechanism

[33] J. H. Ingold, E. Blue, and W. J. Ozeroff, Advan. Energy Conversion 2, 363 (1962), have determined the thermionic work function to be approximately 4.1 eV. If the photoelectric and thermionic surface potential barriers are assumed to be equal, the vacuum level should lie 4.1 eV about the Fermi level at −0.617 eV in Fig. 10.

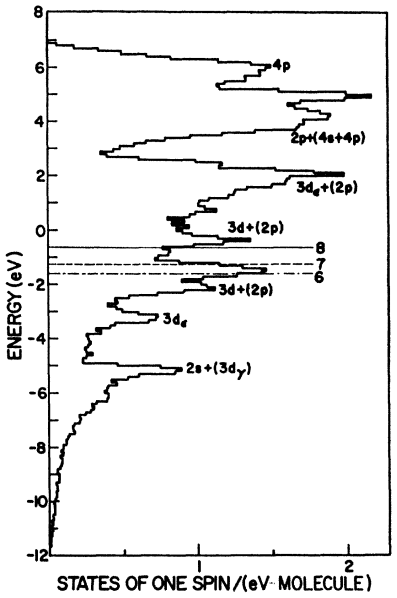

FIG. 13. The density-of-states histogram for TiC calculated from the band structure illustrated in Fig. 10. Major contributions to the peaks are indicated; less important contributions are in parentheses.

explains the behavior observed in Fig. 4. Changes in the photoemission may also occur through perturbations of the energy bands involved in the transitions as carbon is removed from the lattice; such changes may become important at large deviations from stoichiometry.

Another composition-dependent contribution to the photoemission may be expected, on the basis of this band structure, to result from $2s$-$4p$ transitions associated with the transition $^1\Gamma_1$-$^2\Gamma_{15}$. This contribution should have a diffuse threshold near 9 eV, rise to a peak near 15 eV, and fall again to zero at a photon energy equal to the band gap at the center of the zone, 18.3 eV. The peak near 15 eV in Fig. 5 appears to satisfy this description, but little is known of its dependence on carbon content.

The optical conductivity associated with transitions which give rise to the composition-dependent photoemission should likewise depend on the carbon content. This expectation is borne out by experimental observations, but the behavior has not yet been subject to quantitative examination.

C. Density of States and Transport Properties

The density-of-states curve shown in Fig. 13 is a histogram constructed from the distribution in energy of the eigenvalues calculated at points equivalent to 16 384 points uniformly distributed in the Brillouin zone. The preliminary distribution was arranged in 0.1-eV intervals and then smoothed[25] by averaging the number of eigenvalues in three adjoining intervals before plotting in Fig. 13. The horizontal lines mark the levels to which the bands would be filled (in the rigid-band approximation) by the indicated number of electrons. Although the density of states at the Fermi level of stoichiometric TiC (8 electrons) is somewhat greater than the experimental data suggest, the shape of the curve is otherwise in rather good agreement with that predicted from studies of the magnetic susceptibility[34,35] and thermoelectric power.[10] [Note the minimum near the Fermi level of stoichiometric TiC and the sharp rise to a maximum near the Fermi level of $TiC_{0.5}$ (6 electrons).]

If the rigid-band approximation implied by the preceding discussion remained true as carbon atoms were removed from the lattice, the Fermi level would quickly fall below $\Gamma_{25'}$, the bottom of the band which appears to provide the principal mobile charge carriers.[36] Studies of the Hall coefficient[37] suggest, to the contrary, that the number of mobile carriers remains constant or even increases somewhat for small departures from stoichiometry. If the conduction band shape (effective mass) is not drastically altered in the process of removing carbon from the lattice, the Fermi energy measured relative to the bottom of the band must, therefore, increase also. In particular, if the mobile carriers are in two bands of almost identical mass, as appears to be the case for the $\Gamma_{25'}$ minimum,[38] and if these carriers have the free electron mass, then, according to the Hall effect measurements, their Fermi energy at 77°K *increases* from 0.34 eV when $x=0.969$ ($n_c=0.037$ electrons/molecule) to 0.45 eV when $x=0.928$ ($n_c=0.056$ electrons/molecule). This behavior can be understood if the rigid band approximation is relaxed enough to permit the position of the $\Gamma_{25'}$ level to vary with the concentration of carbon. The assumption is not unreasonable in that the $\Gamma_{25'}$ level is influenced strongly by the two-center integral $dd\pi M$, which, in turn, is sensitive to the potential generated by the carbon atoms.[22] As carbon atoms are removed from the lattice, the effective value of $dd\pi M$ is decreased and $\Gamma_{25'}$ is lowered as a result, possibly by a significant amount since $dE(\Gamma_{25'})/d(dd\pi M)=4$. Changes elsewhere in the zone due to changes in $dd\pi M$ are less pronounced than at Γ; to a first approximation, then, both the Fermi level and the bottom of the conduction band are ex-

[34] H. Bittner and H. Goretzki, Monatsh. Chem. **93**, 1000 (1962).
[35] H. Bittner, H. Goretzki, F. Benesovsky, and H. Nowotny, Monatsh. Chem. **94**, 518 (1963).
[36] The absence of a pronounced piezoresistive effect [W. S. Williams, Bull. Am. Phys. Soc. **7**, 174 (1962)] suggests that other pockets of mobile carriers elsewhere in the present band structure are probably spurious; small variations in certain of the two-center integrals may permit these pockets to be eliminated.
[37] W. S. Williams (Ref. 2). See also J. Piper, Ref. 22, p. 29.
[38] Although the principal conduction band was discussed in Ref. 10 as a single s-like band, in analogy with the discussion of the transition metals by Mott and Jones [*Theory of the Properties of Metals and Alloys* (Dover Publications, New York, 1958), pp. 267, 313], the present assignment of the conduction band minimum to the $\Gamma_{25'}$ level implies that the conduction electrons have primarily $3d_\epsilon$ character. The interpretation of the thermoelectric power of TiC_x remains as in Ref. 10, but now depends on scattering of mobile $3d$ electrons into relatively heavy overlapping $3d$ states.

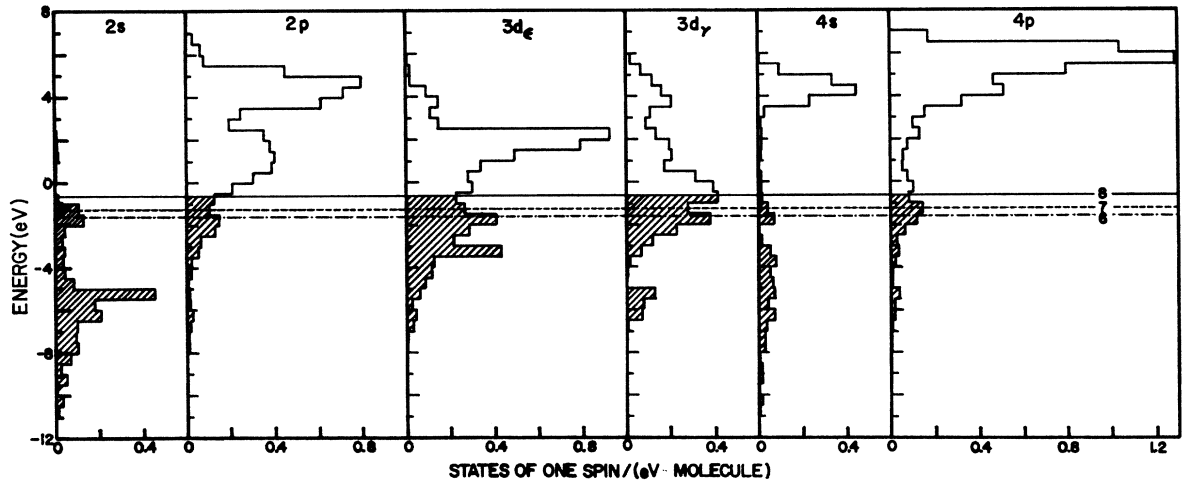

FIG. 14. Density-of-states histograms for the separate atomic states from which the band structure of Fig. 10 was calculated.

pected to move down through the other bands as carbon atoms are removed from the lattice. To agree with observations of the Hall coefficient, the $\Gamma_{25'}$ level must be lowered somewhat faster than is the Fermi level.

Although this proposal provides a plausible explanation for the composition dependence of the transport properties, it is obviously an oversimplification of the problem, neglecting the perturbation of bands other than the conduction band as carbon is removed. A quantitative discussion must await more detailed information regarding the energy bands near the Fermi level.

D. Distribution of Atomic States

The density-of-states curve in Fig. 13 has indicated on it the origin of some of its prominent features to emphasize the complex nature of the structure. This distribution of atomic states is illustrated more clearly in the separate histograms of Fig. 14. Wider intervals, of 0.5 eV, were used (without smoothing) in the latter histograms because of the small number of points in each interval. Resemblances will be noted between these histograms for the $3d_\epsilon$ and $3d_\gamma$ density of states and the curves given by Costa and Conte[22]; differences must be attributed, in part, to interaction of the $3d$ states with other atomic states, interactions not considered by Costa and Conte.

According to Fig. 14, the atomic configurations in TiC are approximately $(2s)^2(2p)^{3/4}$ for carbon and $(3d_\epsilon)^{9/4}(3d_\gamma)^{7/4}(4s)^{3/4}(4p)^{1/2}$ for titanium. Thus, electrons have been lost from carbon $2p$ states to titanium states with a consequent spatial separation of charge which is only imperfectly shielded by the small concentration of mobile charge carriers present in TiC. Although the amount of charge transferred from the carbon to titanium atomic spheres may not be so large as the $1\frac{1}{4}$ electrons suggested by the atomic configurations (because of the overlap of titanium wave functions onto carbon atom sites), the small interatomic separation in TiC($\cong$2.16 Å) may, nevertheless, lead to significant ionic interactions. The degree of ionicity remains undetermined, since the $2p$ states in the present band structure are higher than necessary to be consistent with a *uniform* distribution of the $\pm 1\frac{1}{4}$ electrons over atomic spheres equal in radius to half the interatomic separation. Since the true charge distribution is unlikely to be this simple, the primary criteria for locating the $2p$ levels have been derived from the optical properties instead of from the rather less accurate estimate of equilibrium lattice potentials. It would be highly instructive to determine the charge distribution experimentally through careful studies of x-ray diffraction patterns. Unfortunately, the experimental difficulties in doing so are formidable for TiC.

If the simple model used before to discuss the transport properties is approximately correct, it leads to an interesting description of the behavior of TiC when carbon atoms are removed from the lattice. In this view, the fcc array of titanium atoms is not greatly disturbed by the removal of carbon atoms except that the $dd\pi M$ integral is decreased, as discussed above, and the occupancy of the titanium states are changed. Figure 15 shows the number of electrons in titanium states as a function of composition, TiC_x. As carbon atoms are removed, the number of electrons in titanium states diminishes toward the normal value for titanium metal at a composition near $TiC_{0.5}$. When the titanium atoms have their normal complement of electrons and have an adequate number of vacant carbon sites nearby, it may be expected that they will participate in a phase transformation and revert to the usual *hcp* structure of metallic titanium. Such a transformation is, in fact, observed near the composition $TiC_{0.6}$.[39]

[39] I. Cadoff and J. P. Nielsen, J. Metals 5, 248 (1953).

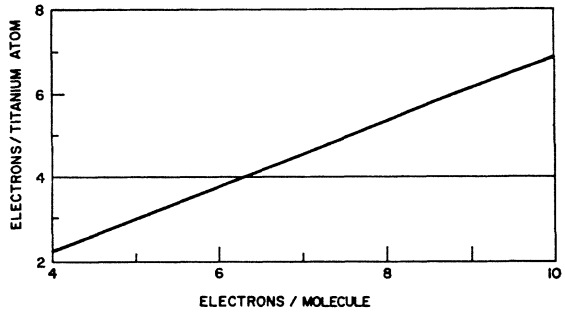

FIG. 15. The number of electrons in titanium atomic states as a function of the total number of electrons per molecule of TiC (rigid-band approximation).

E. Comparison with Related Work

Bilz's[3] calculations imply a greater applicability of the rigid-band concept than our results would support. Differences in the one-electron energies[23] of the $2p$ states suggest that, neglecting other considerations, the level ${}^1\Gamma_{15}$ should be lowered relative to its position in TiC by approximately $2\frac{1}{2}$ eV for TiN and approximately $5\frac{1}{4}$ eV for TiO. Changes in the interactions between atomic states as their relative positions are varied can be expected to have a marked influence on the properties of the three compounds, much more so for TiO than for TiN, since the peak density of the $2p$ states will lie closer to the $3d$ states in the oxide than it will in the nitride. Furthermore, transfer of electrons between metal and nonmetal states will change direction when the $2p$ states are lowered sufficiently; the oxide can be expected to have a much more fully occupied $2p$ band and behave more as an ionic solid than does either the carbide or the nitride. Thus, although the rigid-band model may suggest the response to be anticipated from small departures from stoichiometry or from small additions of related compounds, it no longer appears reasonable to expect a single band structure to provide an adequate representation of TiC, TiN, and TiO.

It should be noted that the density-of-states curve *estimated* by Bilz from his band structure shows far fewer sharp features than does the present result. Although the present band structure is certainly subject to refinement, it seems probable that much of the structure in the density-of-states curve will remain. Arguments based primarily on the smoothly varying curve of Bilz must, therefore, be viewed with caution.

The work of Costa and Conte[22] on the $3d$ band of TiC was based on the tight-binding approximation also but followed Fletcher's[40] approach in incorporating contributions to the local potential from remote lattice sites. Costa and Conte's results emphasized the great influence of neighboring carbon atom core potentials on metal $dd\pi$ interactions and thereby helped resolve the apparent conflict between two of the prominent views[41] of the role played by carbon atoms in determining the bonding of substances like TiC. The calculations by Costa and Conte demonstrated that, despite the slightly increased metal-metal separation in the carbide, the metal-metal interactions may be much stronger than in the parent metal because of the presence of carbon atoms in the region of $3d_\epsilon$ orbital overlap. Costa and Conte calculated separate contributions to the Fletcher parameter A_4 (which is equivalent to $dd\pi$ in the two-center approximation only) and determined that the carbon potentials contributed 0.809 eV, or three-quarters of the total, 1.082 eV. In the present calculation, this effect has been allowed for in a crude way, while retaining the two-center formalism, by increasing $dd\pi$ from the value 0.1 eV, estimated by Bilz from values appropriate for copper and nickel, to 0.55 eV. In addition, interactions neglected by Costa and Conte between $3d$ states and other atomic states of the system have been included in the new calculation. If the resulting band structure is applicable, it must be concluded that essentially covalent metal-metal, carbon-metal, and carbon-carbon interactions play an important role in the bonding, together with an ionic component of some importance which results from the uncompensated electron transfer from carbon to metal states. This model for the bonding in TiC includes the aspects considered important in most of the previous discussions of this problem and reconciles, in large part, conflicts among them.

During the course of this work, a new study of the band structures of TiC, TiN, and TiO was reported by Ern and Switendick,[4] using the augmented-plane-wave approach as adapted by Switendick[42] for structures which contain two different types of atoms in the unit cell. Their results differ substantially from those obtained here and, without extensive modifications, they appear incapable of explaining the optical data on which our calculations rely. Two aspects, in particular, should be noted. First, the $4s$ states of titanium are placed much higher and the $2p$ states of carbon much lower relative to the d bands than in the present band structure. The origin of the discrepancy is not immediately obvious, but it appears possible that inapplicable assumptions have been made in the four basic considerations[42] pertinent to the augmented-plane-wave (APW) calculation: (1) the core potentials (dependent on electronic configurations within the atoms), (2) the constant potential, V_c, between the APW spheres, (3) the ionicity of each atom in the unit cell, and (4) the

[40] G. C. Fletcher, Proc. Phys. Soc. (London) **A65**, 192 (1952).

[41] R. E. Rundle, Acta Cryst. **1**, 180 (1948), suggested that metal-metal bonding was not important in compounds like TiC; the band structure of Bilz (Ref. 3) appears to provide support for his arguments. The opposite point of view, in support of metal-metal bonding, has been presented by R. Kiessling, Met. Rev. **2**, 77 (1957), D. A. Robins, Powder Met. **1/2**, 172 (1958), E. Dempsey, Phil. Mag. **8**, 285 (1963), and P. Costa and R. R. Conte, Ref. 22. J. Piper has discussed certain aspects of the problem recently (Ref. 22, p. 29).

[42] A. C. Switendick, Ref. 32.

APW sphere radii (dependent on the core potentials and on the Madelung displacements).

Ern and Switendick determined the core potentials from self-consistent solutions of the Hartree-Fock-Slater equations using neutral atom configurations: $(3d)^2(4s)^2$ for titanium and $(2s)^2(2p)^2$ for carbon. No Madelung correction was applied in determing V_c from the common potential at the contact of the APW spheres. The present results suggest, instead, that the electronic configurations should be more nearly: $(3d)^4(4s)^{3/4}(4p)^{1/2}$ for titanium and $(2s)^2(2p)^{3/4}$ for carbon. These differences in the electronic configurations imply different core potentials and different ionicities which, in turn, influence the APW sphere radii and the parameter V_c. The appropriate value to be used for V_c is, however, somewhat uncertain in the APW calculation and, although the lower bands and core states are relatively insensitive to changes in this parameter, the upper bands are critically affected. Thus, Scop[43] found it necessary to make empirical adjustments of V_c in order to have the calculated band gaps of AgCl and AgBr agree with the values observed optically. Furthermore, the choices of electronic configurations and, therefore, the core potentials, also have an important bearing on the relative positions of the bands even in monatomic solids, as Mattheiss[44] has demonstrated for the energy bands of vanadium.

Ern and Switendick determined the charges associated with each electronic state within the APW spheres and compared them with the charges contained in equivalent spheres around free atoms having the electronic configurations they had assumed initially. The results appear to be internally consistent, but the agreement may be partially fortuitous if, as the present results suggest, their assumed electronic configurations and APW sphere radii are in error.

In addition to differences in the relative positions of the bands, a second important difference between the two calculations will be noted in the shapes of the bands: near the center of the zone in Ern and Switendick's band structure, the $2p$ bands from Γ_{15} show strong positive curvature and the $3d_\epsilon$ bands from $\Gamma_{25'}$ show negative curvature. As Fig. 10 shows, the present band structure exhibits largely opposite curvature in both cases. Thus Ern and Switendick's calculation indicates the presence of hole pockets at the center of the band instead of the electron valleys of the present band structure. Experimental evidence[2,10] strongly supports the view that the majority charge carriers are electrons, but it must be acknowledged that residual uncertainties remain because of the presence of other electron and hole pockets elsewhere in the zone in both structures.

It seems likely that the curvature of the bands determined by Ern and Switendick is merely a consequence of the proximity of the $2p$ and $3d$ bands, as suggested originally for a different problem by Krumhansl[45] and confirmed recently for the silver halides by Bassani, Knox, and Fowler.[46] Appropriate adjustment of V_c, of the core potentials, and of the Madelung displacement may separate the APW bands and thereby modify their shapes (and positions) to conform better with experimental observations.

It must be concluded that, although there are inadequacies in the present band structure, its principal characteristics are well supported both by the optical data presented here and by other experimental evidence. It is hoped that these results may provide an incentive and serve as a basis for additional, more sophisticated studies of TiC and related compounds.

ACKNOWLEDGMENTS

The authors gratefully acknowledge the advice and encouragement provided by Professor P. L. Hartman during measurements of the optical properties. Various aspects of the work have benefited from discussions with other members of the staff of Parma Technical Center and with Professor J. A. Krumhansl, Professor R. Smoluchowski, and Professor C. S. Smith. B. L. Kopfstein of the Parma Computer Service group expedited the calculations and P. A. Drobnak provided able assistance throughout. Finally, it is a pleasure to acknowledge indebtedness to Professor J. W. McClure for his invaluable assistance with calculations of the band structure and optical properties and for his advice and encouragement throughout these studies.

[43] P. M. Scop, Ref. 32.
[44] L. F. Mattheiss, Phys. Rev. **134**, A970 (1964).
[45] J. A. Krumhansl, in *Photoconductivity Conference*, edited by R. G. Breckenridge *et al.* (John Wiley & Sons, Inc., New York, 1956), p. 450.
[46] F. Bassani, R. S. Knox, and W. B. Fowler, Phys. Rev. **137**, A1217 (1965).